Theory of the upper critical field of superconducting superlattices

S. Takahashi and M. Tachiki
The Research Institute for Iron, Steel and Other Metals, Tohoku University, Katahira, Sendai 980, Japan
(Received 18 November 1985)

The upper critical field of superconducting superlattices is calculated by taking account of spatial variations of the following quantities of conduction electrons: the density of states, the diffusion constant, the attractive interaction constant responsible for superconductivity, and the spin polarization. For applied magnetic fields parallel to the layers, these spatial variations cause a dimensional crossover in the temperature dependence of the upper critical field $H_{c2||}$. The spatial variation of the density of states is most important for the effect of the dimensional crossover observed in Nb/Cu superlattices. For applied magnetic fields perpendicular to layers, a new type of crossover is predicted in the temperature dependence of $H_{c2\perp}$ for superlattices composed of a high-H_{c2} material and a low-H_{c2} material. The anisotropic spin polarization of conduction electrons induced by applied magnetic fields explains the anomalous behavior of H_{c2} observed in V/Ni superlattices.

I. INTRODUCTION

Artificially prepared superlattices, such as Nb/Ge,[1] Nb/Cu,[2] V/Ag,[3] and V/Ni,[4] are a new class of superconducting materials. These superlattices exhibit novel physical properties when the superconducting films with the thickness comparable to the superconducting coherence length are separated by a suitable metal, semiconductor, or insulator so as to establish the high degree of anisotropy in the superlattices. Of particular interest is the behavior of the upper critical field H_{c2}. The temperature dependence of the upper critical field parallel to the layers $H_{c2||}$ shows dimensional crossover, i.e., it changes from the bulk three-dimensional to the two-dimensional dependence at the particular temperature. The behavior of H_{c2} and its anisotropy are quite sensitive to the strength and nature of the coupling between the superconducting layers.

In Nb/Ge superlattices, the superconducting Nb layers are coupled by the Josephson tunneling through the insulating Ge layers with the thickness of the order of 10 Å. A Josephson tunneling model has been proposed by Lawrence and Doniach[5] and later studied extensively by Klemm, Luther, and Beasley.[6] This model explains successfully the temperature dependence of the upper critical field of Nb/Ge superlattice.[1]

In Nb/Cu and V/Ag superlattices, on the other hand, the superconducting layers are coupled through normal conducting Cu or Ag layers by the proximity effect. The relatively strong coupling between the superconducting layers in the superlattices allows a large normal metal thickness of the order of 100 Å. Banerjee *et al.*[7] and Chun *et al.*[8] have investigated systematically the temperature dependence of the parallel and perpendicular critical fields $H_{c2||}$ and $H_{c2\perp}$ by varying the thickness of Nb and Cu layers in Nb/Cu superlattices. When the ratio of $H_{c2||}$ to $H_{c2\perp}$ at low temperatures is plotted as a function of the layer thickness a peak appears at the layer thickness comparable to the superconducting coherence length.[7] Around the peak the dimensional crossover from the three-dimensional to the two-dimensional behavior occurs in the temperature dependence of $H_{c2||}$. A similar crossover was observed by Kanoda *et al.* in V/Ag superlattices.[3]

The V/Ni superlattice is an example of artificially prepared magnetic superconductor. The magnetic effect of Ni layers on superconductivity is controlled by changing the thickness of Ni layers. When the thickness of Ni layers is decreased, the Curie temperature of Ni decreases to lower than the superconducting transition temperature of V and vanishes in the vicinity of 10 Å. Below this film thickness the strong pair breaking effect due to the spin fluctuation and the spin polarization in the Ni layers is weakened enough so that the V layers couple through the Ni layers by the proximity effect. Homma *et al.* measured the upper critical field of the V/Ni superlattices and found the anomalous temperature dependence of H_{c2}. Close to the superconducting transition temperature the parallel upper critical field $H_{c2||}$ is smaller than the perpendicular critical field $H_{c2\perp}$, while at low temperatures the anisotropy of H_{c2} reverts to the normal one, i.e., $H_{c2||} > H_{c2\perp}$.[4] To explain this anomalous behavior of H_{c2} we consider the pair breaking mechanism due to the spin polarization of conduction electrons in the Ni layers. According to the proximity effect, the conduction electrons in the Ni layers becomes superconductive. At high temperatures near the superconducting transition temperature the vortices extend over many layers and the superconductivity is affected by the spin polarization. The spin polarization of the conduction electrons in the Ni layers is anisotropic; the spin polarization induced by the parallel magnetic field is larger than that by the perpendicular magnetic field. This is inferred from the anisotropy of magnetization measured in Mo/Ni superlattices.[9] Therefore, the effect of the pair breaking is larger in the parallel magnetic field than in the perpendicular magnetic field. When the size of the vortices becomes less than the separation of the superconducting layers at low temperatures, the cores of vortices are preferentially situated in the Ni layers for the parallel magnetic field. Therefore, at

low temperatures, the anisotropy of H_{c2} reverts to the normal one as observed in Nb/Ge, Nb/Cu, and V/Ag superlattices.

For superconductor/normal-metal superlattices such as Nb/Cu and V/Ag we take into account the spatial variation of the electron density of states, the diffusion constant of conduction electrons, and the BCS electron-electron interaction constant. All of these quantities are assumed to be uniform in each metal layer. For superlattices of superconductor/normal-metal with the large spin susceptibility such as V/Ni, we consider the effect of the spin polarization of conduction electrons in the magnetic layers in addition to the effects mentioned above. The preliminary results have been presented elsewhere.[10]

In Sec. II we present a general formulation for the upper critical field of the superlattices and derive the equation to determine the parallel and perpendicular upper critical fields. The results of numerical calculations of the upper critical fields for superconductor/normal-metal superlattices are presented in Sec. III. Numerical results for superlattices of superconductor/normal-metal with the large spin susceptibility are given in Sec. IV.

II. FORMULATION

We consider a superlattice composed of two kinds of metal layers. For simplicity, we assume that the electron density of states $N(\mathbf{r})$, the diffusion constant of conduction electrons $D(\mathbf{r})$, the BCS electron-electron interaction constant $V(\mathbf{r})$, and the mean-field exchange potential due to the spin polarization of conduction electrons $I_m(\mathbf{r})$ are uniform inside the layers and change discontinuously at the interfaces.

When the phase transition at H_{c2} is of second order, the superconducting order parameter $\Delta(\mathbf{r})$ is governed by the linearized integral equation[11–13]

$$\Delta(\mathbf{r})=V(\mathbf{r})k_BT\sum_{\omega}\int d^3r'\,Q_{\omega}(\mathbf{r},\mathbf{r}')\Delta(\mathbf{r}')\ , \tag{1}$$

where the kernel is

$$Q_{\omega}(\mathbf{r},\mathbf{r}')=-\tfrac{1}{2}\sum_{\mu,\nu}\sum_{\sigma,\tau}\sum_{\lambda,\kappa}\frac{\phi_{\nu}^{*}(\mathbf{r}',\sigma)\rho_{\sigma\tau}\phi_{\mu}^{*}(\mathbf{r}',\tau)\phi_{\mu}(\mathbf{r},\lambda)\rho_{\lambda\kappa}\phi_{\nu}(\mathbf{r},\kappa)}{(\xi_{\mu}-i\omega)(\xi_{\nu}+i\omega)}\ , \tag{2}$$

where $\omega=(2l+1)\pi k_BT$, l being integers, and $\rho=i\sigma_y,\sigma_y$ being the Pauli matrix. The wave function $\phi_{\mu}(\mathbf{r},\tau)$ is calculated from the Schrödinger equation

$$\sum_{\tau}\left[-\frac{1}{2m}\left[\hbar\nabla-\frac{ie}{c}\mathbf{A}(\mathbf{r})\right]^2\delta_{\sigma\tau}+u_{\sigma\tau}(\mathbf{r})\right]\phi_{\mu}(\mathbf{r},\tau)=\xi_{\mu}\phi_{\mu}(\mathbf{r},\sigma)\ , \tag{3}$$

where μ is a quantum number, τ is the spin coordinate, $\mathbf{A}(\mathbf{r})$ is the vector potential, and $u_{\sigma\tau}(\mathbf{r})$ is given by

$$u_{\sigma\tau}(\mathbf{r})=u_0(\mathbf{r})\delta_{\sigma\tau}+I_m(\mathbf{r})(\sigma_z)_{\sigma\tau}\ . \tag{4}$$

In (4) the first term is an ordinary one-electron potential including the scattering potential due to impurities and boundaries, and the second term is the mean-field exchange potential from the spin polarization of conduction electrons.

Now we introduce a function[12,14]

$$g_{\mu}(\mathbf{r},\mathbf{r}';\Omega)=-\tfrac{1}{2}\sum_{\nu}\sum_{\sigma,\tau}\sum_{\lambda,\kappa}\phi_{\nu}^{*}(\mathbf{r}',\sigma)\rho_{\sigma\tau}\phi_{\mu}^{*}(\mathbf{r}',\tau)\phi_{\mu}(\mathbf{r},\lambda)\rho_{\lambda\kappa}\phi_{\nu}(\mathbf{r},\kappa)\delta(\Omega+\xi_{\mu}-\xi_{\nu})\ . \tag{5}$$

The Fourier transform of $g_{\mu}(\mathbf{r},\mathbf{r}';\Omega)$,

$$g_{\mu}(\mathbf{r},\mathbf{r}';t)=\int d\Omega\,g_{\mu}(\mathbf{r},\mathbf{r}';\Omega)e^{-i\Omega t}\ , \tag{6}$$

is a one-electron correlation function, namely

$$g_{\mu}(\mathbf{r},\mathbf{r}';t)=-\tfrac{1}{2}\langle\mu\,|\,K^{\dagger}(t)\delta(\mathbf{r}-\mathbf{r}(t))\delta(\mathbf{r}'-\mathbf{r}(0))K(0)\,|\,\mu\rangle\ , \tag{7}$$

where $K(t)$ and $\mathbf{r}(t)$ are Heisenberg operators describing the time evolution, respectively, of the time-reversal operator $K=-i\sigma_yC$ (with C the complex-conjugation operator) and the position operator for one electron. $|\,\mu\rangle$ is the Dirac's ket vector whose corresponding $(\mathbf{r},\tau)$ representation is $\phi_{\mu}(\mathbf{r},\tau)$.

Using (5)–(7), we rewrite the kernel $Q_{\omega}(\mathbf{r},\mathbf{r}')$ of (2) in terms of the correlation function

$$Q_{\omega}(\mathbf{r},\mathbf{r}')=\sum_{\sigma}\int d\xi\int d\Omega\int\frac{dt}{2\pi}\frac{e^{i\Omega t}g_{\xi}^{\sigma}(\mathbf{r},\mathbf{r}';t)}{(\xi+\Omega+i\omega)(\xi-i\omega)}\ , \tag{8}$$

where

$$g_{\xi}^{\sigma}(\mathbf{r},\mathbf{r}';t)=\sum_{n}\delta(\xi-\xi_{\mu})g_{\mu}(\mathbf{r},\mathbf{r}';t),\quad \mu=(n,\sigma)\ . \tag{9}$$

In (8) the dominant contribution to the integral comes from small values of ξ, and thus $g_{\xi}^{\sigma}(\mathbf{r},\mathbf{r}';t)$ can be approximated by $g_{\xi=0}^{\sigma}(\mathbf{r},\mathbf{r}';t)$, where $\xi=0$ corresponds to the Fermi energy. Then, we have

$$Q_{\omega}(\mathbf{r},\mathbf{r}')\simeq 2\pi\sum_{\sigma}\int_0^{\infty}dt\,e^{-2|\omega|t}g_{\xi=0}^{\sigma}(\mathbf{r},\mathbf{r}';t)\ , \tag{10}$$

For $t\to 0$, $g_{\xi=0}^{\sigma}(\mathbf{r},\mathbf{r}';t)$ reduces to the initial condition

$$\lim_{t\to 0}g_{\xi=0}^{\sigma}(\mathbf{r},\mathbf{r}';t)=\delta(\mathbf{r}-\mathbf{r}')\sum_{n}\delta(\xi_{\mu})\sum_{\tau}|\,\phi_{\mu}(r\tau)\,|^2$$
$$=\tfrac{1}{2}\delta(\mathbf{r}-\mathbf{r}')N(\mathbf{r})\ , \tag{11}$$

where $N(\mathbf{r})$ is the position-dependent density of states at the Fermi level. Here we assumed that the density of state is constant near the Fermi level.

The operator $K(t)$ in (7) satisfies the equation of motion[12]

$$\frac{\partial}{\partial t}K(t)=\frac{2i}{\hbar}I_m(\mathbf{r}(t))\sigma_z K(t)-i\frac{d\theta(t)}{dt}K(t)\ , \tag{12}$$

$$\theta(t)\simeq\frac{2e}{\hbar c}\int_{\mathbf{r}(0)}^{\mathbf{r}(t)}d\mathbf{s}\cdot\mathbf{A}(\mathbf{s})\ , \tag{13}$$

where the expression of $\theta(t)$ results from the semiclassical phase approximation.

The probability density of finding a particle at the position $\mathbf{r}$ satisfies the continuity equation

$$\frac{\partial}{\partial t}\delta(\mathbf{r}-\mathbf{r}(t))+\nabla\cdot\mathbf{i}(\mathbf{r},\mathbf{r}(t))=0\ ,$$

where $\mathbf{i}(\mathbf{r},\mathbf{r}(t))$ is the current operator of the particle. When the motion of $\mathbf{r}(t)$ is controlled by a diffusion (random walk) process, $\mathbf{i}(\mathbf{r},\mathbf{r}(t))$ is given by $-D(\mathbf{r})\nabla\delta(\mathbf{r}-\mathbf{r}(t))$ where $D=\frac{1}{3}v_F l$ is the diffusion constant, v_F and l being the Fermi velocity and the mean free path in the normal state, respectively. Therefore, $\delta(\mathbf{r}-\mathbf{r}(t))$ obeys the familiar diffusion equation

$$\frac{\partial}{\partial t}\delta(\mathbf{r}-\mathbf{r}(t))=D(\mathbf{r})\nabla^2\delta(\mathbf{r}-\mathbf{r}(t))\ . \tag{14}$$

Using (7), (12), and (14), we obtain the gauge-invariant form of the equation of motion for $g^{\tau}_{\xi=0}(\mathbf{r},\mathbf{r}';t)$

$$\left[\hbar\frac{\partial}{\partial t}+2iI_m(\mathbf{r})(\sigma_z)_{\tau\tau}\right]g^{\tau}_{\xi=0}(\mathbf{r},\mathbf{r}';t)=\hbar D(\mathbf{r})\left[\nabla-\frac{2ie}{\hbar c}\mathbf{A}(\mathbf{r})\right]^2 g^{\tau}_{\xi=0}(\mathbf{r},\mathbf{r}';t)\quad(t>0)\ . \tag{15}$$

With the aid of the equation of motion (15) we can construct a differential equation for $Q_\omega(\mathbf{r},\mathbf{r}')$. Let us introduce an auxiliary quantity $R_\omega(\mathbf{r},\mathbf{r}')$ defined by

$$R_\omega(\mathbf{r},\mathbf{r}')=2\pi\sum_{\tau}\int_0^\infty dt\,(\sigma_z)_{\tau\tau}g^{\tau}_{\xi=0}(\mathbf{r},\mathbf{r}';t)e^{-2|\omega|t}\ . \tag{16}$$

By using (11) and (15) we can show that $Q_\omega(\mathbf{r},\mathbf{r}')$ and $R_\omega(\mathbf{r},\mathbf{r}')$ satisfy the following differential equations:

$$[2|\omega|+L(\nabla)]Q_\omega(\mathbf{r},\mathbf{r}')+2iI_m(\mathbf{r})R_\omega(\mathbf{r},\mathbf{r}')=2\pi\delta(\mathbf{r}-\mathbf{r}')N(\mathbf{r})\ , \tag{17}$$

$$[2|\omega|+L(\nabla)]R_\omega(\mathbf{r},\mathbf{r}')+2iI_m(\mathbf{r})Q_\omega(\mathbf{r},\mathbf{r}')=0\ , \tag{18}$$

where the linear operator $L(\nabla)$ is defined by

$$L(\nabla)=-\hbar D(\mathbf{r})\left[\nabla-\frac{2ie}{\hbar c}\mathbf{A}(\mathbf{r})\right]^2\ . \tag{19}$$

In order to solve (17) and (18), we introduce eigenfunctions $\psi_\lambda(\mathbf{r})$ and eigenvalues ε_λ of the operator $L(\nabla)$,

$$L(\nabla)\psi_\lambda(\mathbf{r})=\varepsilon_\lambda\psi_\lambda(\mathbf{r})\ , \tag{20}$$

with appropriate boundary conditions at the interfaces mentioned later. By expanding $Q_\omega(\mathbf{r},\mathbf{r}')$ and $R_\omega(\mathbf{r},\mathbf{r}')$ in terms of $\psi_\lambda(\mathbf{r})$'s

$$Q_\omega(\mathbf{r},\mathbf{r}')=[N(\mathbf{r})N(\mathbf{r}')]^{1/2}\sum_{\lambda,\lambda'}a_{\lambda\lambda'}\psi^*_{\lambda'}(\mathbf{r}')\psi_\lambda(\mathbf{r})\ , \tag{21}$$

$$R_\omega(\mathbf{r},\mathbf{r}')=[N(\mathbf{r})N(\mathbf{r}')]^{1/2}\sum_{\lambda,\lambda'}b_{\lambda\lambda'}\psi^*_{\lambda'}(\mathbf{r}')\psi_\lambda(\mathbf{r})\ , \tag{22}$$

and inserting (21) and (22) into (17) and (18), we have the equations for the expansion coefficients $a_{\lambda\lambda'}$ and $b_{\lambda\lambda'}$

$$(2|\omega|+\varepsilon_\lambda)a_{\lambda\lambda'}+2i\sum_\zeta\langle\lambda|I_m|\zeta\rangle b_{\zeta\lambda'}=2\pi\delta_{\lambda\lambda'}\ , \tag{23}$$

$$(2|\omega|+\varepsilon_\lambda)b_{\lambda\lambda'}+2i\sum_\zeta\langle\lambda|I_m|\zeta\rangle a_{\zeta\lambda'}=0\ , \tag{24}$$

where the matrix element $\langle\lambda|I_m|\zeta\rangle$ is defined by

$$\langle\lambda|I_m|\zeta\rangle=\int d^3r\,\psi^*_\lambda(\mathbf{r})I_m(\mathbf{r})\psi_\zeta(\mathbf{r})\ . \tag{25}$$

Solving (23) and (24) and inserting $a_{\lambda\lambda'}$ into (21) we obtain the expression for $Q_\omega(\mathbf{r},\mathbf{r}')$

$$Q_\omega(\mathbf{r},\mathbf{r}')=2\pi[N(\mathbf{r})N(\mathbf{r}')]^{1/2}\sum_{\lambda,\lambda'}\psi_\lambda(\mathbf{r})\Gamma^{-1}_{\lambda\lambda'}(\omega)\psi^*_{\lambda'}(\mathbf{r}')\ . \tag{26}$$

In (26), $\Gamma^{-1}_{\lambda\lambda'}(\omega)$ is the inverse matrix element of $\Gamma(\omega)$. The matrix element of $\Gamma(\omega)$ is given by

$$\Gamma_{\lambda\lambda'}(\omega)=(2|\omega|+\varepsilon_\lambda)\delta_{\lambda\lambda'}+4\sum_\zeta\frac{\langle\lambda|I_m|\zeta\rangle\langle\zeta|I_m|\lambda'\rangle}{2|\omega|+\varepsilon_\zeta}\ . \tag{27}$$

If we make use of (26), our starting integral equation (1) is written as

$$F(\mathbf{r})=2\pi T[N(\mathbf{r})]^{1/2}\sum_\omega\sum_{\lambda,\lambda'}\psi_\lambda(\mathbf{r})\Gamma^{-1}_{\lambda\lambda'}(\omega)\int d^3r'\psi^*_{\lambda'}(\mathbf{r}')V(\mathbf{r}')[N(\mathbf{r}')]^{1/2}F(\mathbf{r}')\ , \tag{28}$$

where $F(\mathbf{r})=\Delta(\mathbf{r})/V(\mathbf{r})$ is the pair function. By expanding $F(\mathbf{r})$ in terms of $\psi_\lambda(\mathbf{r})$,

$$F(\mathbf{r})=[N(\mathbf{r})]^{1/2}\sum_\lambda c_\lambda\psi_\lambda(\mathbf{r})\ , \tag{29}$$

we convert (28) to a matrix equation of c_λ's. If we require that this matrix equation has nontrivial solutions, the following secular equation must vanish:

$$\det\left|\delta_{\lambda\lambda'}-2\pi T\sum_\omega\sum_\zeta\Gamma^{-1}_{\lambda\zeta}(\omega)\langle\zeta|VN|\lambda'\rangle\right|=0\ , \tag{30}$$

where

$$\langle\zeta \mid VN \mid \lambda'\rangle = \int d^3r\, \psi_\zeta^*(\mathbf{r}) V(\mathbf{r}) N(\mathbf{r}) \psi_{\lambda'}(\mathbf{r}) . \quad (31)$$

The quantities $\Gamma_{\lambda\zeta}$ and $\langle\zeta \mid VN \mid \lambda'\rangle$ include the vector potential. From a solution of the secular equation (30) the upper critical field is determined as a function of temperature.

We must now pick the appropriate boundary conditions at the interfaces. De Gennes has derived the boundary conditions that the quantities[14]

$$\Delta(\mathbf{r})/N(\mathbf{r})V(\mathbf{r}) = F(\mathbf{r})/N(\mathbf{r}) \quad (32)$$

and

$$\frac{D(\mathbf{r})}{V(\mathbf{r})}\left[\nabla - \frac{2ie}{\hbar c}\mathbf{A}(\mathbf{r})\right]\Delta(\mathbf{r}) = D(\mathbf{r})\left[\nabla - \frac{2ie}{\hbar c}\mathbf{A}(\mathbf{r})\right]F(\mathbf{r}) \quad (33)$$

are continuous at the interfaces. When solving the eigenvalue equation (20), we impose on $[N(\mathbf{r})]^{1/2}\psi_\lambda(\mathbf{r})$ the same boundary conditions as those for $F(\mathbf{r})$. Then, from relation (29), $F(\mathbf{r})$ automatically satisfies the boundary conditions (32) and (33). Equation (30) has many solutions under the boundary conditions. The highest magnetic-field solution among the solutions corresponds to the upper critical field. In the next section we calculate the upper critical fields when the magnetic field is applied parallel and perpendicular to the layers of superlattices.

III. SUPERCONDUCTOR/NORMAL-METAL SUPERLATTICES

Let us consider a superlattice composed of alternating layers of a normal metal and a superconductor, with thickness of d_N and d_S, respectively. The z axis is taken perpendicular to the layers. The geometrical configuration is schematically illustrated in Fig. 1. The electron density of states $N(z)$, the diffusion constant $D(z)$, and the electron-electron interaction constant $V(z)$ are assumed to be uniform in the layers, and are denoted by N_S, D_S, and V_S for the superconducting layers (S layers), and N_N, D_N, and V_N for the normal-metal layers (N layers), respectively. In this paper, the term of the normal-metal layers is understood to include the layers of weak superconductors. In order to elucidate the effect of the spatial variation of $N(z)$, $D(z)$, and $V(z)$ on the upper critical field, we examine these effects separately.

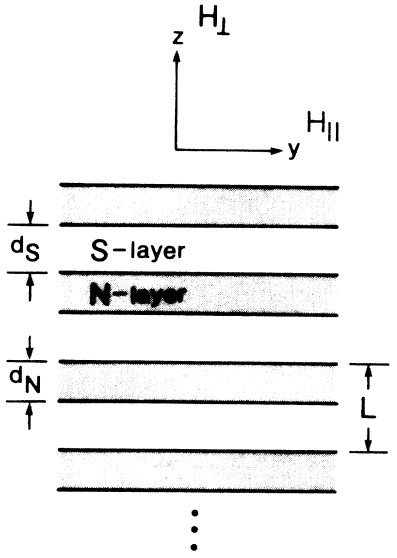

FIG. 1. Geometrical configuration of a superlattice.

A. Effect of $N(z)$ on H_{c2}

We first consider the effect of the spatial variation of the density of states $N(z)$ on the upper critical field. The density of states in the superconducting (S) and normal (N) layers is assumed to be of the form

$$N(z) = \begin{cases} N_S & \text{for } nL - d_S/2 < z < nL + d_S/2 \text{ for } S \text{ layers} \\ N_N & \text{for } nL + d_S/2 < z < (n+1)L - d_S/2 \text{ for } N \text{ layers} , \end{cases} \quad (34)$$

with n being integer S and $L = d_S + d_N$. We assume $V_S = V_N$ ($\equiv V$) and $D_S = D_N$ ($\equiv D$). We calculate the eigenvalues ε_λ and the eigenfunctions $\psi_\lambda(\mathbf{r})$ of Eq. (20) under the boundary condition that

$$N(z)[(d/dz)\ln\psi_\lambda(\mathbf{r}) - (2ie/\hbar c)\mathbf{A}_z(\mathbf{r})]$$

is continuous at the interfaces. Using the ground-state wave function $\psi_G(\mathbf{r})$ with the lowest eigenvalue ε_G as a variational function, we calculate the secular equation (30) as

$$\ln\left[\frac{T}{T_c}\right] + \Psi\left[\frac{1}{2} + \frac{\varepsilon_G}{4\pi k_B T}\right] - \Psi\left(\tfrac{1}{2}\right) = 0 , \quad (35)$$

where

$$T_c = 1.134\omega_D \exp\left[-\frac{\int d^3r \mid \psi_G(\mathbf{r}) \mid^2}{\int d^3r\, \psi_G^*(\mathbf{r}) N(z) V(z) \psi_G(\mathbf{r})}\right] , \quad (36)$$

where T_c is the superconducting transition temperature of the superlattice, $\Psi(z)$ is the digamma function, and ω_D is the Debye temperature. Among ε_λ's, ε_G gives the highest magnetic field which corresponds to H_{c2}. Detailed calculations for ε_G and $\psi_G(\mathbf{r})$ are presented in Appendixes A and B. In the following we confine ourselves to the superlattices with small values of N_N/N_S, since the above variational calculation is exact in the limit of $N_N/N_S \to 0$. This case may correspond to the Nb/Ge superlattice. The results may also be applicable to the Nb/Cu and V/Ag superlattices, since the densities of states of Cu and Ag are much smaller than those of Nb and V.

In Fig. 2 we show the temperature dependence of the calculated upper critical fields $H_{c2\parallel}$ and $H_{c2\perp}$ for several values of the layer thickness $d = d_S = d_N$. The ratio N_N/N_S is taken to be 0.15. The solid and dashed curves denote the parallel ($H_{c2\parallel}$) and perpendicular ($H_{c2\perp}$) upper critical fields, respectively. As seen in Fig. 2, for the

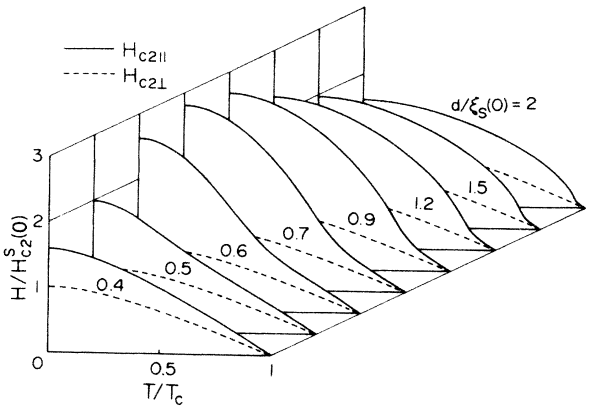

FIG. 2. Temperature dependence of the parallel (solid curves) and perpendicular (dashed curves) upper critical fields of the superlattices with the spatial variation of the density of states $N(z)$ shown for several values of layer thickness $d=d_S=d_N$. We take $N_N/N_S=0.15$, $V_S=V_N$, and $D_S=D_N$. In the figure $H^S_{c2}(0)$ is the upper critical field of the bulk superconductor of the S layer material and $\xi_S(0)=[\phi_0/2\pi H^S_{c2}(0)]^{1/2}$.

values of $d/\xi_S(0)$ from 0.6 to 2, $H_{c2\parallel}$ sharply increases with a concave curvature. This temperature dependence may show the occurrence of the dimensional crossover; at high temperatures near T_c, $H_{c2\parallel}$ varies linearly in T like H_{c2} in a three-dimensional superconductor, and at low temperatures it varies in a square-root fashion in T like H_{c2} in a two-dimensional superconductor. This temperature dependence originates from the fact that in the T-linear region the pair function $F(\mathbf{r})$ spreads over many layers, whereas at low temperatures it is confined almost in a single S layer. When the value of $d/\xi_S(0)$ increases, the crossover temperature at which $H_{c2\parallel}$ turns upwards shifts to a higher temperature. For $d/\xi_S(0)=0.4$, $H_{c2\parallel}$ behaves like an ordinary bulk superconductor. The perpendicular upper critical field $H_{c2\perp}$ is almost independent

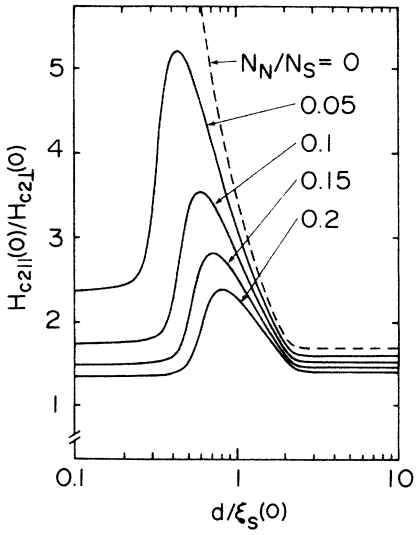

FIG. 3. Ratio of $H_{c2\parallel}$ to $H_{c2\perp}$ at $T=0$ K as a function of the layer thickness $d=d_S=d_N$. The parameters are the same as those in Fig. 2.

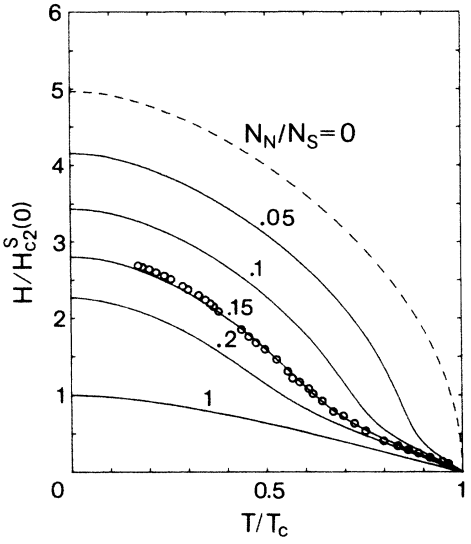

FIG. 4. Temperature dependence of the calculated upper critical fields $H_{c2\parallel}$ shown for several values of N_N/N_S. We take $d=d_S=d_N=0.70\xi_S(0)$, $V_S=V_N$, and $D_S=D_N$. The open circles are the experimental values of the Nb/Cu superlattice with 200 Å obtained by Banerjee *et al* (Ref. 7).

of the layer thickness d.

Figure 3 shows the ratio of $H_{c2\parallel}$ to $H_{c2\perp}$ at $T=0$ K as a function of layer thickness d. The solid curves indicate the ratios of $H_{c2\parallel}/H_{c2\perp}$ for the values of $N_N/N_S=0.05$, 0.1, 0.15, and 0.2. A peak appears in each curve at the thickness slightly below $\xi_S(0)$. For the large thickness, $H_{c2\parallel}$ tends to H_{c3} due to the surface superconductivity. The dashed curve for $N_N/N_S=0$ tends to the well-known value 1.695 of $H_{c3}/H_{c2\perp}$ for the large thickness.[15] Banerjee *et al.* observed a sharp peak of $H_{c2\parallel}/H_{c2\perp}$ between 100 and 300 Å in the Nb/Cu superlattices.[7] The experimental result may be explained by the above mechanism.

The temperature dependence of the parallel upper critical field $H_{c2\parallel}$ is shown for several values of N_N/N_S in Fig. 4. The layer thickness is taken to be $d/\xi_S(0)=0.7$. As seen from the figure, $H_{c2\parallel}$ shows the dimensional

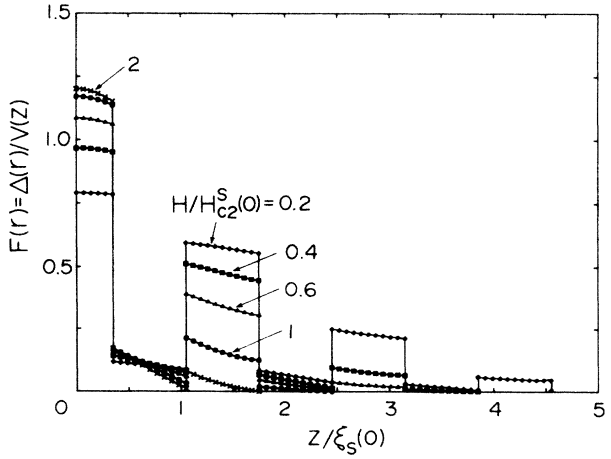

FIG. 5. Spatial variation of the pair function $F(\mathbf{r})$ in the superlattice with $N_N/N_S=0.15$ and several values of $H_{c2\parallel}$ (see Fig. 4).

crossover. The open circles in the figure show the experimental data of the Nb/Cu superlattice with thickness 200 Å obtained by Banerjee *et al.*[7] The calculated $H_{c2\parallel}$ for $N_N/N_S=0.15$ is in good agreement with the experimental values. The value of $N_N/N_S=0.15$ is very close to the experimental value $\gamma_{Cu}/\gamma_{Nb}\simeq 0.16$, where γ_{Cu} and γ_{Nb} are, respectively, the coefficients of the normal-state electronic specific heat of Cu and Nb.[16] From the value of $d/\xi_S(0)=0.7$, $\xi_S(0)$ is estimated to be 286 Å which is comparable to the coherence length of Nb. In the above calculation we assume that $D_{Cu}=D_{Nb}$. Since the relevant layer thickness d is much less than the mean free path of bulk Cu, the mean free path may be limited by the layer thickness. The mean free path of bulk Nb is comparable to the layer thickness d. Therefore, we assumed $D_{Cu}/D_{Nb}=1$ in the analysis of the experimental data. Figure 5 shows the spatial variation of the superconducting pair function $F(\mathbf{r})$ in the superlattice with $N_N/N_S=0.15$ for several values of $H_{c2\parallel}$. In the cases of $H/H_{c2}^S(0)=0.2$ and 0.4 the pair function $F(\mathbf{r})$ spreads over many layers so that the superlattice behaves like a three-dimensional bulk superconductor. On the other hand, for $H/H_{c2}^S(0)=2$ the pair function is almost confined within a single S layer so that the superlattice behaves like a thin film superconductor.

B. Effect of $D(z)$ on H_{c2}

Next we consider the upper critical field of the superlattice with the spatial variation of the diffusion constant

$$D(z)=\begin{cases} D_S & \text{for } nL-d_S/2<z<nL+d_S/2 \text{ for } S \text{ layers} \\ D_N & \text{for } nL+d_S/2<z<(n+1)L-d_S/2 \text{ for } N \text{ layers} . \end{cases} \tag{37}$$

The other parameters are constant in space. Since $V(z)N(z)$ $[\equiv N(0)V]$ is constant, the matrix element $\langle\lambda\,|\,VN\,|\,\lambda'\rangle$ in (30) has the form $\delta_{\lambda\lambda'}N(0)V$. The secular equation (30) then reduces to a simple form

$$\ln\left[\frac{T}{T_c}\right]+\Psi\left[\frac{1}{2}+\frac{\varepsilon_G}{4\pi k_B T}\right]-\Psi(\tfrac{1}{2})=0 , \tag{38}$$

where ε_G is the lowest eigenvalue of Eq. (20). ε_G and the corresponding eigenfunction $\psi_G(\mathbf{r})$ are calculated under the boundary condition that

$$D(z)[(d/dz)\ln\psi_G(\mathbf{r})-(\hbar c/zie)\mathbf{A}_z(\mathbf{r})]$$

is continuous at the interfaces. The calculations for ε_G and $\psi_G(\mathbf{r})$ are shown in Appendixes A and B. We should note that $\psi_G(\mathbf{r})$ is nothing but the pair function $F(\mathbf{r})$ for $c_G=1/[N(0)]^{1/2}$ in (29).

In Fig. 6 we show the calculated parallel upper critical field $H_{c2\parallel}$ of the superlattice with the spatial variation of the diffusion constant. The thicknesses of the S and N layers are taken to be $d/\xi_S(0)=0.75$. As seen from Fig. 6, the crossover from the three-dimensional to the two-dimensional behavior occurs for the large values of D_N/D_S.

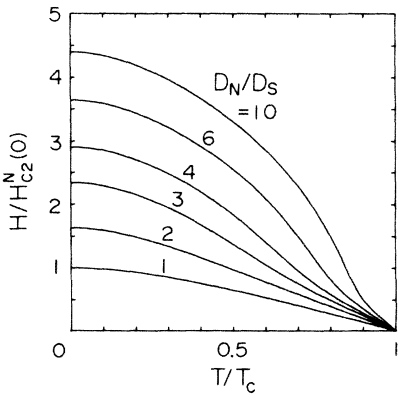

FIG. 6. Temperature dependence of the parallel upper critical field $H_{c2\parallel}$ of the superlattice with the spatial variation of the diffusion constant $D(z)$ shown for several values of D_N/D_S. We take $d=d_S=d_N=0.75\xi_S(0)$, $V_S=V_N$, and $N_S=N_N$. In the figure $H_{c2}^N(0)$ is the upper critical field of the bulk superconductor of the N-layer material.

The perpendicular upper critical field $H_{c2\perp}$ is calculated in the following way. As shown in Appendix B, the lowest eigenvalue ε_G in (38) is calculated from the equation

$$D_S k_S \tan(\tfrac{1}{2}k_S d_S)=D_N\kappa_N \tanh(\tfrac{1}{2}\kappa_N d_N) , \tag{39}$$

with

$$k_S=\frac{1}{\xi_N(0)}\left[\left[\frac{D_N\varepsilon_G}{D_S\varepsilon_N}-1\right]\frac{H}{H_{c2}^N(0)}\right]^{1/2} , \tag{40}$$

$$\kappa_N=\frac{1}{\xi_N(0)}\left[\left[1-\frac{\varepsilon_G}{\varepsilon_N}\right]\frac{H}{H_{c2}^N(0)}\right]^{1/2} , \tag{41}$$

where $\varepsilon_N=(2e/\hbar c)\hbar D_N H$, $H_{c2}^N(0)$ is the upper critical field of the bulk superconductor of the N-layer material, and $\xi_N(0)=[\phi_0/2\pi H_{c2}^N(0)]^{1/2}$. In the N layers the pair function damps with the damping constant κ_N from the interfaces and in the S layers the pair function oscillates with the wave number k_S. Similar calculations were performed by Biagi *et al.*[17]

Figure 7 shows the perpendicular upper critical field $H_{c2\perp}$ as a function of temperature. The parameters are the same as those of Fig. 6. As seen from the figure, the remarkable upturn appears in $H_{c2\perp}$, especially for the large values of D_N/D_S. In the vicinity of the transition temperature the pair function is almost uniform in the direction of the vortices. The ratio of the initial slope of $H_{c2\perp}$ to that of H_{c2}^N is limited by the value of 2, because it is given by

$$(2D_N/D_S)/(1+D_N/D_S) .$$

When the temperature decreases, the pair function in the S layers increases rapidly and is confined in the S layers.

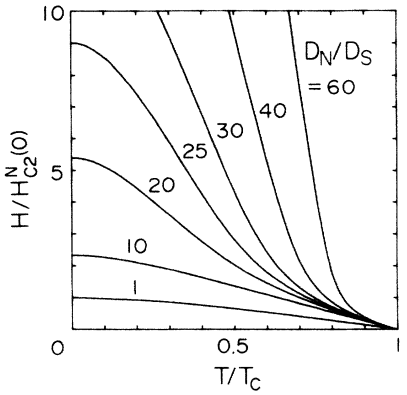

FIG. 7. Temperature dependence of the perpendicular upper critical field $H_{c2\perp}$ shown for several values of D_N/D_S. The parameters are the same as those in Fig. 6.

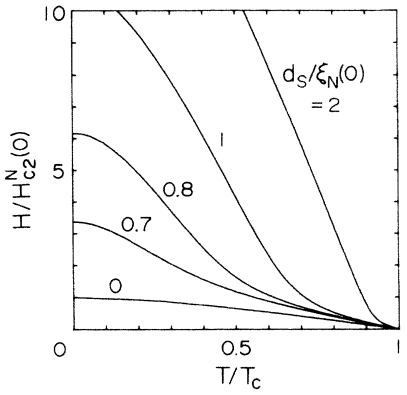

FIG. 8. Temperature dependence of $H_{c2\perp}$ shown for several values of $d_S/\xi_N(0)$ and $d_N/\xi_N(0)=2$. The parameters are taken to be $N_N/N_S=1$ and $D_N/D_S=20$.

As a result, the temperature dependence of $H_{c2\perp}$ is almost the same as that of the S layers.

Figure 8 shows the temperature dependence of the perpendicular upper critical field $H_{c2\perp}$ for several values of the S-layer thickness. The N-layer thickness is fixed at $d_N/\xi_N(0)=2$. As seen from the Fig. 8, $H_{c2\perp}$ is quite sensitive to the value of $d_S/\xi_N(0)$. Figure 9 shows the temperature dependence of $H_{c2\perp}$ for several values of the N layer thickness. The S layer thickness is fixed at $d_S/\xi_N(0)=0.75$. When the S-layer thickness is fixed, $H_{c2\perp}$ is insensitive to $d_N/\xi_N(0)$.

Let us consider the spatial variation of the density of states in addition to the diffusion constant. The lowest eigenvalue ε_G in (35) is determined from the equation (see Appendix B)

$$D_S N_S k_S \tan(\tfrac{1}{2}k_S d_S)=D_N N_N \kappa_N \tanh(\tfrac{1}{2}\kappa_N d_N)\ , \quad (42)$$

where k_S and κ_N are given by (40) and (41). Using (40)–(42) we calculate the perpendicular upper critical field $H_{c2\perp}$. In Fig. 10 we show $H_{c2\perp}$ for $D_N/D_S=25$ and several values of N_S/N_N. Other parameters are the same as those in Fig. 7. As seen from the figure, for small values of N_S/N_N, a sharp upturn curvature appears. In this case, the pair function is confined in the N layers above the temperature at which the upturn occurs, whereas below the temperature the pair function is confined in the S layers.

C. Effect of $V(z)$ on H_{c2}

We consider the upper critical field of the superlattice with the spatial variation of the electron-electron interaction constant $V(z)$, which is assumed of the form

$$V(z)=\begin{cases} V_S & \text{for } nL-d_S/2<z<nL+d_S/2 \text{ for } S \text{ layers} \\ V_N & \text{for } nL+d_S/2<z<(n+1)L-d_S/2 \text{ for } N \text{ layers}\ . \end{cases} \quad (43)$$

$N_S=N_N$ [$\equiv N(0)$] and $D_S=D_N$ ($\equiv D$) are assumed.

When a magnetic field is applied parallel to the layers, the secular equation to determine the parallel upper critical field $H_{c2\parallel}$ is given by

$$\det\left|\delta_{nm}+\left[\Psi\left(\frac{1}{2}+\frac{\varepsilon_n}{4\pi k_B T}\right)-\Psi(\tfrac{1}{2})+\ln\left(\frac{T}{T_S}\right)\right.\right.$$
$$\left.\left.-\frac{1}{V_S N(0)}\right]N(0)\langle n\mid V\mid m\rangle\right|=0\ , \quad (44)$$

where T_S is the transition temperature of the bulk superconductor of the S layer material, $\epsilon_n=(2n+1)(2e/\hbar c)\hbar DH$, $\Psi(z)$ is the digamma function, and $\langle n\mid V\mid m\rangle$ is defined by

$$\langle n\mid V\mid m\rangle=\frac{\sqrt{2}}{\xi(T)}\int_{-\infty}^{\infty}dz w_n\left[\frac{\sqrt{2}}{\xi(T)}(z-z_0)\right]$$
$$\times V(z) w_m\left[\frac{\sqrt{2}}{\xi(T)}(z-z_0)\right]\ , \quad (45)$$

where $\xi(T)=(\phi_0/2\pi H)^{1/2}$ and $w_n(z)$ is the Weber function. For the values of z_0 and T, the secular equation (44) gives a discrete set of values of H. Among the magnetic fields, we take the largest value. Then, varying z_0 we calculate the maximum value of H, which corresponds to $H_{c2\parallel}$.

The perpendicular upper critical field $H_{c2\perp}$ is calculated from the secular equation

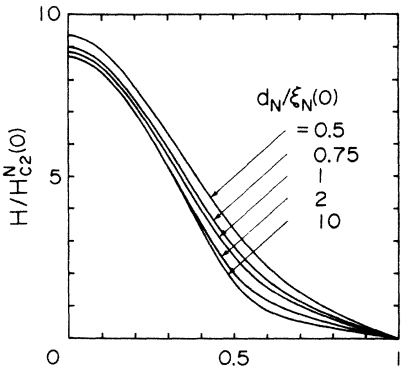

FIG. 9. Temperature dependence of $H_{c2\perp}$ for several values of $d_N/\xi_N(0)$ and $d_S/\xi_N(0)=0.75$. The parameters are taken to be $N_N/N_S=1$ and $D_N/D_S=25$.

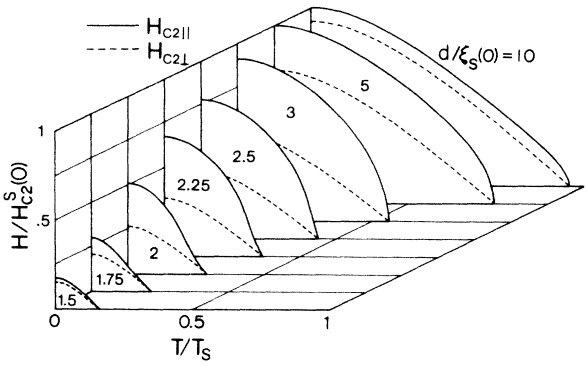

FIG. 11. Temperature dependence of the parallel (solid curves) and perpendicular (dashed curves) upper critical fields of the superlattice with the spatial variation of the BCS interaction constant $V(z)$ is shown for several values of the layer thickness $d=d_S=d_N$. We take $V_SN_S=0.3$, $V_NN_N=0$, $N_S=N_N$, and $D_S=D_N$.

$$\det\left|\delta_{GG'}+\left[\Psi\left(\frac{1}{2}+\frac{\varepsilon_{n=0}+\hbar DG'^2}{4\pi k_BT}\right)-\Psi\left(\tfrac{1}{2}\right)+\ln\left(\frac{T}{T_S}\right)-\frac{1}{V_SN(0)}\right]N(0)V_{G-G'}\right|=0\,, \tag{46}$$

where $G=2\pi n/L$ is the reciprocal vector of the superlattice, and V_G is the Fourier component of $V(z)$ and given by

$$V_G=V_N\delta_{G0}+(V_S-V_N)(d_S/L)\sin(Gd_S/2)/(Gd_S/2)\,.$$

In Fig. 11 we show the temperature dependence of the upper critical fields for several values of the layer thickness $d=d_S=d_N$. The parameters $V_SN_S=0.3$ and $V_NN_N=0$ are used. The solid curves show the parallel upper critical fields $H_{c2\parallel}$ and the dashed curves show the perpendicular upper critical fields $H_{c2\perp}$. The temperature dependence of $H_{c2\parallel}$ for $d/\xi_S(0)=5$ and 10 behaves like a two-dimensional film near T_c and that of bulk well below T_c. For $d/\xi_S(0)=3$, the typical two-dimensional-like behavior, i.e., $H_{c2\parallel}\propto(1-T/T_c)^{1/2}$ is seen in the whole temperature range. These temperature dependences originate from the fact that the S layers are decoupled and behave independently because the penetration depth of the superconducting order parameter into the N layer is less than the thickness of the N layers. When the film thickness becomes smaller, a small upturn curvature appears in the temperature dependence of $H_{c2\parallel}$. When $d/\xi_N(0)$ is near unity, the superconducting order parameters spread over many layers so that the superlattice behaves like a three-dimensional superconductor.

Figure 12 shows the ratio of $H_{c2\parallel}$ to $H_{c2\perp}$ at $T=0$ K (solid curve) and the superconducting transition temperature (dash-dotted curve) as a function of the layer thickness $d=d_S=d_N$. The parameters are the same as those in

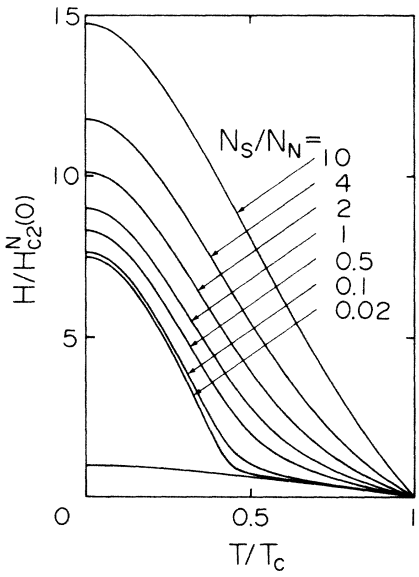

FIG. 10. Temperature dependence of the perpendicular upper critical fields $H_{c2\perp}$ with the spatial variation of the density of states $N(z)$ and the diffusion constant $D(z)$ is shown for $D_N/D_S=25$ and several values of N_S/N_N. Other parameters are the same as those in Fig. 7.

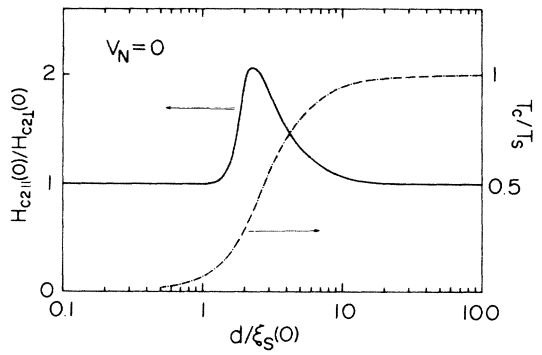

FIG. 12. Ratio of $H_{c2\parallel}$ to $H_{c2\perp}$ at $T=0$ K (solid curve) and the superconducting transition temperature of the superlattice (dash-dotted curve) are shown as a function of the layer thickness d. The parameters are the same as those in Fig. 11.

Fig. 11. At the layer thickness $d/\xi_S(0)\sim 2.3$ a peak appears in the solid curve. It is seen from the Fig. 12 that the peak of $H_{c2\parallel}/H_{c2\perp}$ appears in the transition region where the superconducting transition temperature T_c changes from T_S to ~ 0. Note that for $d/\xi_S(0)\ll 1$, for which the pair function $F(\mathbf{r})$ should be uniform in the superlattice; (46) has a solution of so-called Cooper limit for the transition temperature.[18]

The superconductive coupling between the S layers changes with the electron-electron interaction constant V_N in the N layers. In Fig. 13 we show the upper critical fields of $H_{c2\parallel}$ and $H_{c2\perp}$ as a function of temperature for several values of V_N/V_S. For the small values of V_N/V_S, the superconducting transition temperature decreases due to the proximity effect. The anisotropy of the upper critical fields increases with decreasing V_N/V_S.

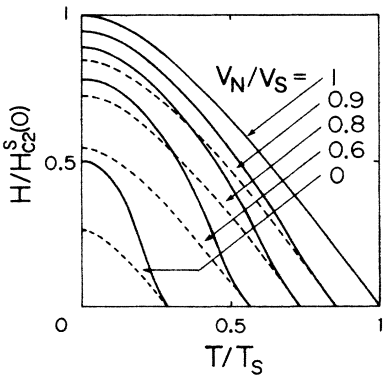

FIG. 13. Temperature dependence of $H_{c2\parallel}$ (solid curves) and $H_{c2\perp}$ (dashed curves) shown for several values of V_N/V_S. The layer thickness is taken to be $d/\xi_S(0)=2$.

IV. SUPERLATTICE OF SUPERCONDUCTOR/NORMAL-METAL WITH LARGE SPIN SUSCEPTIBILITY

In this section we calculate the upper critical field of a superlattice composed of superconducting layers (S layers) and normal-metal layers (N layers) with a large spin susceptibility. The most important effect on the upper critical field comes from the exchange-enhanced spin polarization of conduction electrons in the N layers. When the thickness of the N layers are thin enough, the N-layers become superconductive due to the proximity effect. The spin polarization in the N layers acts as a pair breaker for the Cooper pairs.

The spatial variation of the exchange interaction constant $I(z)$ between conduction electrons is assumed of the form

$$I(z)=\begin{cases}0 & \text{in } nL-d_S/2<z<nL+d_S/2 \text{ for } S \text{ layers}\\ I & \text{in } nL+d_S/2<z<(n+1)L-d_S/2 \text{ for } N \text{ layers}\end{cases}. \tag{47}$$

We take the density of states and the diffusion constant to be constant. Neglecting the spin polarization in the S layers, we consider only the Pauli paramagnetic effect due to the spin polarization in the N layers. When the magnetic field is applied parallel (perpendicular) to the layers, the mean-field exchange potential $I_{m\parallel}(z)$ $[I_{m\perp}(z)]$ due to the spin polarization $m_{\parallel}(z)$ $[m_{\perp}(z)]$ is given by $I_{m\parallel}(z)=I(z)m_{\parallel}(z)$ $[I_{m\perp}(z)=I(z)m_{\perp}(z)]$. We assume that the N layers are in the paramagnetic state down to 0 K. The parallel and perpendicular spin-polarization densities induced by applied magnetic fields are, respectively, given by $m_{\parallel}(z)=\chi_{\parallel}H$ and $m_{\perp}(z)=\chi_{\perp}H$ for the N layers, and $m_{\parallel}(z)=m_{\perp}(z)=0$ for the S layers, where $\chi_{\parallel}$ and $\chi_{\perp}$ are, respectively, the parallel and perpendicular exchange-enhanced paramagnetic susceptibility of the N layers. We neglect the temperature dependence of $\chi_{\parallel}$ and $\chi_{\perp}$. Since $N_S=N_N$ and $D_S=D_N$, the boundary conditions (32) and (33) are reduced to the condition that

$$[(d/dz)\ln F(\mathbf{r})-(2ie/\hbar c)\mathbf{A}_z(\mathbf{r})]$$

is continuous at the interfaces.

From (27) and (30) the parallel upper critical field $H_{c2\parallel}$ is determined from the secular equation

$$\det\left|\delta_{nm}\ln\left[\frac{T}{T_c}\right]-2\pi T\sum_{\omega}\left[\Gamma_{nm}^{-1}(\omega)-\frac{\delta_{nm}}{|\omega|}\right]\right|=0, \tag{48}$$

where n is integer and T_c is the superconducting transition temperature. In (48) $\Gamma^{-1}(\omega)$ is the inverse matrix of $\Gamma(\omega)$, whose matrix element is

$$\Gamma_{nm}(\omega)=(2|\omega|+\varepsilon_n)\delta_{nm}+4I^2H^2\sum_l\frac{\langle n|\chi_{\parallel}|l\rangle\langle l|\chi_{\parallel}|m\rangle}{2|\omega|+\varepsilon_l}, \tag{49}$$

where

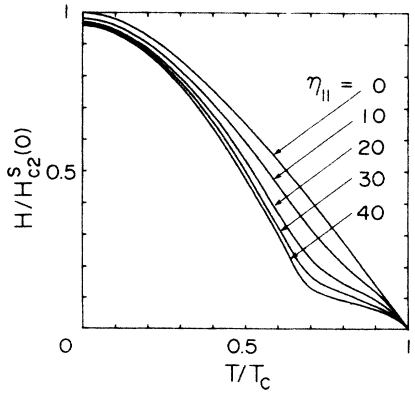

FIG. 14. Temperature dependence of the parallel upper critical field of the superlattice with the spatial variation of the exchange interaction constant between conduction electrons shown for several values of $\eta_{\parallel}$. We take $d_S/\xi_S(0)=4$, $d_N/\xi_S(0)=1$, $V_S=V_N$, $N_S=N_N$, and $D_S=D_N$.

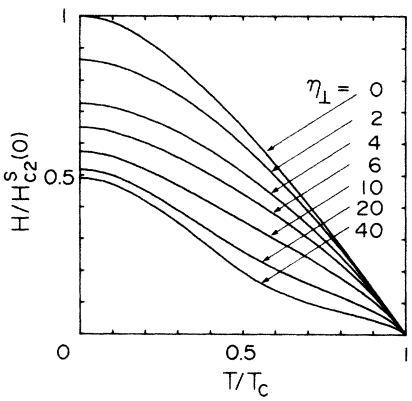

FIG. 15. Temperature dependence of the perpendicular upper critical field of the superlattice is shown for several values of $\eta_\perp$. Other parameters are the same as those in Fig. 14.

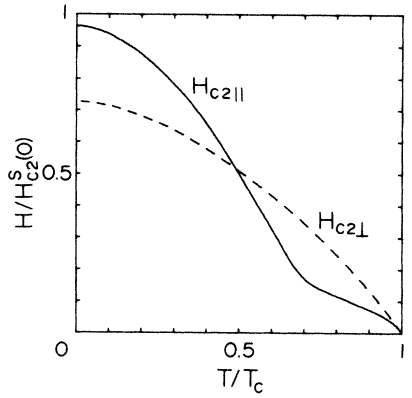

FIG. 16. Parallel (solid curve) and perpendicular (dashed curve) upper critical fields shown as a function of temperature. We take $\eta_\| = 30$ and $\eta_\perp = 4$. Other parameters are the same as those in Figs. 14 and 15.

$$\varepsilon_n = (2n+1)(2e/\hbar c)\hbar DH \ ,$$

D being the diffusion constant, and the matrix element $\langle n \,|\, \chi_\| \,|\, m \rangle$ is given by (45) if $V(z)$ is replaced by $\chi_\|(z)$.

The perpendicular upper critical field $H_{c2\perp}$ is determined from the secular equation

$$\det \left| \delta_{GG'} \ln\left[\frac{T}{T_c}\right] - 2\pi T \sum_\omega \left[\Gamma^{-1}_{GG'}(\omega) - \frac{\delta_{GG'}}{|\omega|} \right] \right| = 0 \ , \tag{50}$$

where $G = 2\pi n/L$ and $\Gamma_{GG'}(\omega)$ is given by

$$\Gamma_{GG'}(\omega) = (2\,|\,\omega\,| + \varepsilon_{n=0} + \hbar DG^2)\delta_{GG'} + 4I^2H^2 \sum_{G''} \frac{\langle G \,|\, \chi_\perp \,|\, G'' \rangle \langle G'' \,|\, \chi_\perp \,|\, G' \rangle}{2\,|\,\omega\,| + \varepsilon_{n=0} + \hbar DG''^2} \ , \tag{51}$$

with

$$\langle G \,|\, \chi_\perp \,|\, G' \rangle = \chi_\perp \{ \delta_{GG'} - (d_S/L)\sin[(G-G')d_S/2]/[(G-G')d_S/2] \} \ .$$

In Fig. 14 we show the calculated parallel upper critical field $H_{c2\|}$ as a function of temperature. The layer thickness is taken to be $d_S/\xi_S(0) = 4$ and $d_N/\xi_S(0) = 1$. We introduce a dimensionless parameter $\eta_\| = I\chi_\| H_{c2}^S(0)/T_c$. As seen from the figure, for large values of $\eta_\|$, $H_{c2\|}$ is strongly suppressed near the transition temperature, since the pair function penetrates into the N layers and suffers from the pair breaking effect due to the spin polarization. At low temperatures the size of the pair function is smaller than the thickness of the S layers, and the pair function is confined within the S layers. Therefore, $H_{c2\|}$ is not depressed at low temperatures.

Figure 15 shows the temperature dependence of the perpendicular upper critical field $H_{c2\perp}$. The parameter $\eta_\perp$ denotes $I\chi_\perp H_{c2}^S(0)/T_c$. For the perpendicular magnetic field, the pair function in the N layers is affected by the pair breaking effect down to 0 K, since the vortex lines penetrate through the S layers. As seen from Fig. 15, a concave curvature appears around $T/T_c = 0.6$ for the large value of $\eta_\perp$.

Figure 16 shows the upper critical field when the spin susceptibility is highly anisotropic. We take $\eta_\| = 30$ and $\eta_\perp = 4$. The solid curve shows $H_{c2\|}$ and the dashed curve shows $H_{c2\perp}$. As seen from the figure, at high temperatures $H_{c2\|}$ is lower than $H_{c2\perp}$ since the spin polarization is larger for the parallel magnetic field. However, at low temperatures $H_{c2\|}$ becomes higher than $H_{c2\perp}$, because he pair function can be confined in the S layers for the parallel magnetic field. Such a crossing behavior has been observed in the V/Ni superlattices by Homma *et al.*[4] The anisotropy of $\eta_\| \gg \eta_\perp$ is inferred from the measurement of magnetization in the Mo/Ni superlattices.[9]

Brodsky found superconductivity in sandwiches of metals such as Au/Cr/Au.[19] Zinn *et al.* investigated the properties of sandwiches of superconductor/ferromagnet such as Pb/EuS.[20]

ACKNOWLEDGMENTS

The authors would like to thank Dr. I. K. Schuller, Dr. H. Homma, Dr. A. J. Fedro, Dr. J. E. Robinson, Dr. K. Kanoda, Professor S. Maekawa, and Dr. T. Koyama for valuable discussions. The authors express special thanks to Mr. K. Miyazato for useful discussions and numerical assistance. This work has been supported by a Grant-in-Aid from the Ministry of Education, Science and Culture, Japan.

APPENDIX A: PARALLEL UPPER CRITICAL FIELD $H_{2c\parallel}$

The magnetic field is applied parallel to the layers in the y direction. We take the vector potential $\mathbf{A}(\mathbf{r})=(Hz,0,0)$ and assume that $\psi_\lambda(\mathbf{r})$ in (20) is of the form

$$\psi_\lambda(\mathbf{r})=e^{ik_x x}w_\lambda([\sqrt{2}/\xi(T)](z-z_0)) \quad (k_y=0)\ , \tag{A1}$$

where $w_\lambda(z)$ is the Weber function, $\xi(T)=(\phi_0/2\pi H)^{1/2}$, and $z_0=(\hbar c/2eH)k_x$. Insertion of (A1) into (20) shows that $w_\lambda(z)$ satisfies the following Weber equation:

$$\left[-\frac{d^2}{dz^2}+\tfrac{1}{4}z^2\right]w_{\lambda_i}(z)=(\lambda_i+\tfrac{1}{2})w_{\lambda_i}(z)\ , \tag{A2}$$

where λ_i has different values λ_S and λ_N when z is the S layers and the N layers, respectively. The eigenvalue ε_λ of (20) is related to λ_S and λ_N through

$$\varepsilon_\lambda=\frac{2\hbar D_S}{\xi^2(T)}(\lambda_S+\tfrac{1}{2})=\frac{2\hbar D_N}{\xi^2(T)}(\lambda_N+\tfrac{1}{2})\ . \tag{A3}$$

The general solution of (A2) in the nth S and N layers can be written as

$$\phi_S^n(z)=\alpha_S^n w_{\lambda_S}([\sqrt{2}/\xi(T)](z-z_0))+\beta_S^n w_{\lambda_S}(-[\sqrt{2}/\xi(T)](z-z_0)) \quad \text{for } z_n^-<z<z_n^+\ , \tag{A4}$$

$$\phi_N^n(z)=\alpha_N^n w_{\lambda_N}([\sqrt{2}/\xi(T)](z-z_0))+\beta_N^n w_{\lambda_N}(-[\sqrt{2}/\xi(T)](z-z_0)) \quad \text{for } z_n^+<z<z_{n+1}^-\ , \tag{A5}$$

where α's and β's are numerical coefficients and $z_n^\pm=\pm d_S/2+n(d_S+d_N)$ are the positions of the interfaces. The coefficients α's and β's and the eigenvalue ε_λ are determined by the boundary conditions

$$N_S D_S\frac{d}{dz}\ln\phi_S^n(z_n^+)=N_N D_N\frac{d}{dz}\ln\phi_N^n(z_n^+)\ , \tag{A6}$$

$$N_S D_S\frac{d}{dz}\ln\phi_S^{n+1}(z_{n+1}^-)=N_N D_N\frac{d}{dz}\ln\phi_N^n(z_{n+1}^-)\ , \tag{A7}$$

and

$$\lim_{z\to\pm\infty}\phi_S^n(z)=\lim_{z\to\pm\infty}\phi_N^n(z)=0\ . \tag{A8}$$

APPENDIX B: PERPENDICULAR UPPER CRITICAL FIELD $H_{c2\perp}$

The magnetic field is applied perpendicular to the layers in the z direction. We take the vector potential $\mathbf{A}(\mathbf{r})=(0,Hx,0)$ and assume $\psi_\lambda(\mathbf{r})$ in (20) of the form

$$\psi_\lambda(\mathbf{r})=\phi(z)w_{n=0}([\sqrt{2}/\xi(T)]x) \quad (k_y=0)\ , \tag{B1}$$

where $w_n(z)$ is the Weber function with integer n and $\xi(T)=(\phi_0/2\pi H)^{1/2}$. We take $n=0$ which corresponds to the lowest eigenvalue. Insertion of (B1) into (20) shows that $\phi(z)$ satisfies the following equations

$$-\frac{d^2}{dz^2}\phi_S(z)=\left[\frac{\varepsilon}{\hbar D_S}-\frac{1}{\xi^2(T)}\right]\phi_S(z) \quad \text{for } S \text{ layers}\ , \tag{B2}$$

$$-\frac{d^2}{dz^2}\phi_N(z)=\left[\frac{\varepsilon}{\hbar D_N}-\frac{1}{\xi^2(T)}\right]\phi_N(z) \quad \text{for } N \text{ layers}\ , \tag{B3}$$

where $\phi_S(z)$ and $\phi_N(z)$ are the wave functions in the S and N layers, respectively. By noting that the derivative of the ground-state wave function at the center of the S and N layers should vanish, we have

$$\phi_S(z)=\alpha_0\cos(k_S z) \quad \text{for } -d_S/2<z<d_S/2\ , \tag{B4}$$

$$\phi_N(z)=\beta_0\cosh\left[\kappa_N\left[z-\frac{d_S+d_N}{2}\right]\right] \quad \text{for } d_S/2<z<d_S/2+d_N\ , \tag{B5}$$

where k_S and κ_N are given in (40) and (41). From the boundary conditions (32) and (33), we have Eqs. (39) and (42) to determine the lowest eigenvalue ε_G.

[1] S. T. Ruggiero, T. W. Barbee, Jr., and M. R. Beasley, Phys. Rev. Lett. **45**, 1299 (1980).

[2] I. K. Schuller, Phys. Rev. Lett. **44**, 1597 (1980).

[3] K. Kanoda, H. Mazaki, T. Yamada, N. Hosoito, and T. Shinjo, Phys. Rev. B **33**, 2052 (1986).

[4] H. Homma, C. S. L. Chun, G.-G. Zheng, and I. K. Schuller, Phys. Rev. B **33**, 3562 (1986); Physica **135B**, 173 (1985).

[5] W. E. Lawrence and S. Doniach, in *Proceedings of the Twelfth International Conference on Low Temperature Physics*, edited by E. Kanda (Academic Press of Japan, Tokyo, 1971), p. 361.

[6] R. A. Klemm, A. Luther, and M. R. Beasely, Phys. Rev. B **12**, 877 (1975).

[7] I. Barnerjee, Q. S. Yang, C. M. Falco, and I. K. Schuller, Phys. Rev. B **28**, 5037 (1983); I. Banerjee and I. K. Schuller, J. Low Temp. Phys. **54**, 501 (1984).

[8] C. S. L. Chun, G.-G. Zheng, J. L. Vicent, and I. K. Schuller, Phys. Rev. B **29**, 4915 (1984).

[9] M. R. Khan, P. Roach, and I. K. Schuller, Solid Thin Films, **122**, 183 (1985).

[10] M. Tachiki and S. Takahasi, Physica **135B**, 178 (1985).

[11] L. P. Gor'kov, Zh. Eksp. Teor. Fiz. **37**, 1407 (1959) [Soviet Phys.—JETP **10**, 998 (1960).

[12]P. G. de Gennes, Phys. Kondens. Mater. **3**, 79 (1964).
[13]N. R. Werthermer, Phys. Rev. **132**, 2440 (1963).
[14]P. G. de Gennes, Rev. Mod. Phys. **36**, 225 (1964).
[15]D. Saint-James and P. G. deGennes, Phys. Lett. **7**, 306 (1963).
[16]I. Banerjee, Q. S. Yang, C. M. Falco, and I. K. Schuller, Solid State Commun. **41**, 805 (1982).
[17]K. R. Biagi, V. G. Kogan, and J. R. Clem, Phys. Rev. B **32**, 7165 (1985).
[18]L. N. Cooper, Phys. Rev. Lett. **6**, 689 (1961).
[19]M. B. Brodsky, J. Magn. Magn. Mater. **35**, 99 (1983).
[20]W. Zinn, B. Saftic, N. Rasula, M. Mirabal, and J. Koehne, J. Magn. Magn. Mater. **35**, 329 (1983).

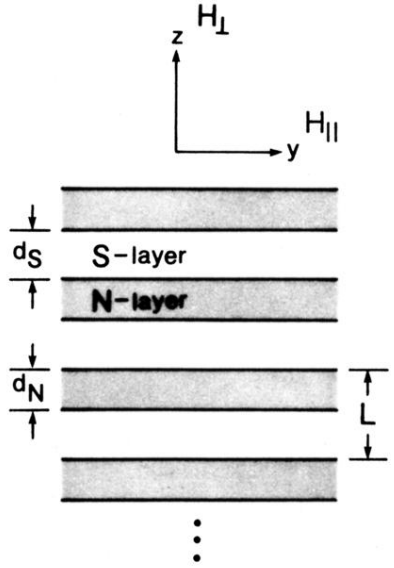

FIG. 1. Geometrical configuration of a superlattice.